Photoelectrocatalytic decolorization of methylene blue using reduced graphene oxide modified TiO_2 on filter paper

Xiaoqiang Li, Jialin Zhang, Zengyuan Pang, Yanan Zhu, Xin Chen, Qian Sun and Yonggui Li

ABSTRACT

In this work, titanium dioxide (TiO_2) was modified with reduced graphene oxide (rGO), and then coated on filter paper to prepare the rGT/FP photoelectrode for the photoelectrocatalytic (PEC) decolorization of methylene blue (MB). The physicochemical properties of the rGT/FP photoelectrode were characterized using scanning electron microscopy (SEM), X-ray diffraction (XRD) analysis and UV-Vis diffuse reflectance spectroscopy (DRS). The decolorization results demonstrated that the photocatalytic (PC) and electrocatalytic (EC) efficiency of the photoelectrode could be significantly improved by the modification of rGO. The improvement of PC and EC efficiency might attribute to the existence of rGO, which could extend the light-harvesting efficiency, promote the photocurrent response value and suppress the charge recombination. Furthermore, the PEC decolorization of MB using the rGT/FP photoelectrode presented higher efficiency than the sum of PC and EC decolorization, indicating the synergistic effect between the photo and electrical energy.

Key words | composite film, dye decolorization, photoelectrocatalysis, reduced graphene oxide, titanium dioxide

Xiaoqiang Li
Jialin Zhang
Zengyuan Pang
Yanan Zhu
Xin Chen
Qian Sun
College of Textiles and Clothing,
Jiangnan University,
Wuxi 214122,
China

Yonggui Li (corresponding author)
Fujian Key Laboratory of Novel Functional Textile Fibers and Materials,
Minjiang University,
Fuzhou 350108,
China
E-mail: *lygwxjd@sina.com*

INTRODUCTION

The photocatalytic (PC) decolorization of organic pollutants using semiconductors has attracted numerous attentions in recent years, because of their use of synchronous light and activated molecules driven in chemical reactions (Hoffmann *et al.* 1995; Chen *et al.* 2010; Wang *et al.* 2018; Takle *et al.* 2019). Among these semiconductors, TiO_2 has been recognized as the most potential PC material, due to its nontoxicity, good biocompatibility, low-cost and excellent PC degradation capability (Chen *et al.* 2018; Sánchez-Rodríguez *et al.* 2018; Sieland *et al.* 2018). Lots of reports had extensively investigated the PC performance of TiO_2 with various nanostructures for decolorizing organic dye effluent (Rajkumar *et al.* 2015; Ren *et al.* 2017; Sathishkumar *et al.* 2017; Subramonian *et al.* 2017). However, the high recombination rate of photogenerated charge carriers of TiO_2 hinders its practical implementation. There are two main strategies to improve the catalytic efficiency of TiO_2, including modifying or doping TiO_2 with other sensitive materials, and using the method of photoelectrocatalysis, which is the combination of photocatalysis and electrocatalysis.

Numerous efforts have been made to vary the chemical composition and structure by doping TiO_2 with ions (Koketsu *et al.* 2017; Smirnova *et al.* 2017; Yan *et al.* 2017), coupling with noble metals (Ghasemi *et al.* 2013; Zhang *et al.* 2013) and forming hybrids with metal sulfides (Mao *et al.* 2013; Lindblad *et al.* 2014; Litke *et al.* 2016; Zhang *et al.* 2018), etc. Graphene, a typical two-dimensional honeycomb carbon material made from the compact accumulation of single layer carbon atoms, has become a new research hotspot since its discovery in 2004, due to its excellent electrical, thermal, mechanical and optical properties (Bolotin *et al.* 2008; Du *et al.* 2008; Liang *et al.* 2010; Zhang *et al.* 2010). Graphene has been widely used in the applications of photocatalysis (Williams *et al.* 2008; Xiang *et al.* 2011), electronic devices (Li *et al.* 2010; Wei *et al.* 2013), micro-nano sensors (Tao *et al.* 2016) and other fields. Recently, many reports have demonstrated the superior performance of nano-semiconductors coupled with reduced graphene oxide (rGO) for enhancing the PC degradation

doi: 10.2166/wst.2019.425

efficiency. For example, Garrafa Galvez *et al.* reported that the rGO/TiO_2 compound possessed the enhanced PC degradation efficiency by a maximum of seven times than that of pristine TiO_2 under UV irradiation (Garrafa-Galvez *et al.* 2019). Kim *et al.* (2017) found that doped TiO_2 nanotube arrays with rGO showed much higher PC degradation efficiency than that of TiO_2 nanotube arrays.

There are many studies that have investigated the PC degradation performance of rGO/TiO_2, with the compound in the various structures of nanoparticle, nanorod or nanotube. Among the different structures, nanoparticles have obtained the most attention, because of the high adsorption capacity and their large specific surface area. However, there are two obvious obstacles that still restrict its application, including difficult recovery from dyed or other polluted waste solutions and confining the form of photocatalysis (Kim & Anderson 1994; Liao & Carter 2013; Zhai *et al.* 2013).

Photoelectrocatalysis has been proven as an efficient technique for pollutant degradation by applying an external bias to the photoelectrode. The photoexcited electrons could be accelerated and separated with holes by the external bias, leading both the electrons and holes to react with reactants (Dai *et al.* 2011; Qin *et al.* 2012).

In this work, the TiO_2 based photoelectrode was prepared and used for photoelectrocatalytic (PEC) decolorization of methylene blue (MB). The reduced graphene oxide was used to modify the TiO_2, to improve the degradation efficiency. Moreover, commercially available filter paper was used as the substrate material for the photoelectrode preparation.

EXPERIMENTAL

Materials

TiO_2 (P25, 80% anatase and 20% rutile) was purchased from Evonik Degussa Co., Ltd. Quantitative filter paper (GB/T1914-2007, Sinopharm Chemical Reagent Co., Ltd) were cut into pieces of 2 cm × 2 cm to obtain the electrode substrate. Ethyl cellulose ($[C_6H_7O_2(OC_2H_5)_3]_n$), and methylene blue (MB) were purchased from Aladdin. Graphite, sulfuric acid, hydrochloric acid (HCl), sodium nitrate ($NaNO_3$), potassium permanganate ($KMnO_4$), and hydrogen peroxide (H_2O_2) were purchased from Sinopharm Chemical Reagent Co., Ltd. All reagents were of analytical grade and used without further purification.

Preparation of rGT/FP photoelectrocatalyst

The composite of rGO and TiO_2 nanoparticles was denoted as rGT and prepared using the hydrothermal method (Guo *et al.* 2019). Details of preparing rGT are provided in the Supplementary Material. The weight ratio of rGO to TiO_2 in the rGT composite was controlled as 5%.

The photoelectrode was obtained by coating rGT onto the filter paper. In detail, 3.0 g ethylcellulose and 0.8 g absolute ethyl alcohol were mixed and stirred to form a clear and viscous fluid; 0.1 g rGT was then added into the fluid to make the rGT mixture. Thereafter, filter paper was coated with the rGT mixture using a doctor-blade method, followed by heat treatment at 60 °C for 10 min to obtain the photoelectrode of rGT/FP. The photoelectrode of TiO_2/filter paper (TiO_2/FP) was also prepared with the same method.

Characterizations

The morphology of samples were observed by scanning electron microscope (SEM, SU1510, HITACHT Ltd, Japan). The X-ray diffraction (XRD) patterns of the samples were recorded via an X-ray diffractometer (D/Max 2200PC, Rigaku Corporation) in the range of 10°–80°, using a nickel filtrated CuKα radiation operated at 28 kV and 20 mA. The element distribution of rGT/FP photoelectrode was analyzed through an energy-dispersive x-ray spectroscopy (EDS, Hitachi S4800). The UV-Vis diffuse reflectance spectroscopy (DRS) were obtained from dry-pressed disk samples using the UV-Vis spectrophotometer (U-4100, Hitachi Ltd, Japan).

Photoelectrochemical measurements

Photoelectrochemical measurements were performed in a conventional three-electrode, single-compartment quartz cell on an Ivium Electrochemical Workstation. A 250 W high-pressure mercury lamp was used to provide the light irradiation. A saturated calomel electrode (SCE) was used as the reference electrode and a Pt plate was used as the counter electrode. 0.1 M Na_2SO_4 was used as the electrolyte. The TiO_2/FP and rGT/FP photoelectrodes were used as the working electrodes, respectively.

Decolorization properties

In the PEC experiments, the rGT/FP was used as the photoelectrode with the dimension of 2.3 cm × 2 cm. The clamping length of the electrode holder was 0.3 cm, and

the effective area of the photoelectrode immersed in the electrolyte was 2 cm × 2 cm. A same-sized platinum foil acted as the cathode. The distance between the two electrodes was 5.0 cm. The light irradiation was supplied by a 250 W high-pressure mercury lamp. The irradiation distance between the lamp and the electrode was set as 10 cm. The electrolyte of 0.05 mol/L KCl was added to increase the conductivity of the MB solution. Prior to irradiation, the two electrodes were vertically aligned in the reactor. Then, 60 mL of the MB solution was added to the reactor and stirred in the dark for 30 min to establish an adsorption-desorption equilibrium. The applied potential in the PEC experiments was controlled by a DC power supply. The decolorization of the MB solution was determined at a wavelength of 664 nm by a UV-Vis spectrophotometer (Shanghai Meipuda Instrument Co., Ltd).

RESULTS AND DISCUSSION

Morphology

The morphology of pristine TiO_2, rGT, TiO_2/FP and rGT/FP was observed by SEM. As shown in Figure 1(a), pristine TiO_2 has a rough surface and loose structure, while a relatively smooth surface and compact structure are presented in rGT (Figure 1(b)), due to the distribution of powdered TiO_2 on the flake rGO. Figure 1(c) and 1(d) show the surface morphology of TiO_2/FP and rGT/FP, respectively. It could be observed that TiO_2/FP possesses a smooth surface with few convex particles, while the rGT/FP exhibits an uneven surface. EDS mapping was used to investigate the distribution of O, C, and Ti elements on rGT/FP, and shown in Figure 2. It can be found that O and C elements are uniformly distributed on the filter paper. The results of EDS demonstrated that the TiO_2 nanoparticles have been homogenously coated onto the filter paper by the doctor blade method.

XRD and UV-Vis analysis

Figure 3(a) shows the XRD patterns that correspond to the samples of pristine TiO_2, rGT, TiO_2/FP and rGT/FP. The diffraction peaks at $2\theta = 25.4°$, 37.8°, 48.1°, 54.0°, 55.1°, 62.7°, 68.8°, 70.3° and 75.1° are indexed to the crystalline planes of anatase TiO_2 (101), (004), (200), (105), (211), (204), (116), (220) and (215), respectively, which correspond to the standard pattern of the anatase crystalline phase of TiO_2 (JPCDS, No. 21-1272) (Almeida & Zanoni 2014). Furthermore, the diffraction peaks at 2θ values of 27.4°, 36.1°, and 41.3° correspond to the rutile TiO_2 (110), (101) and (111) planes (JPCDS, No. 21-1276), respectively. The XRD pattern of rGT sample is quite similar to that of pure TiO_2, while there is not any typical diffraction peak corresponding to rGO, due to the low content of carbon species in the composites (Liu *et al.* 2012; Zhang *et al.* 2009). Therefore, the characteristic peaks of rGO could not be detected on the XRD pattern. The diffraction peaks at 2θ values of 15.13°, 16.90°, and 22.92°, corresponding to the cellulose (JPCDS, No. 50-2241), are strong enough to cover the diffraction peaks of rGT and TiO_2.

Optical characterizations of various samples were then investigated using the UV-Vis diffuse reflectance measurements. As shown in Figure 3(b), pristine TiO_2 samples exhibit very low absorption in the visible region, because of the wide band gap of TiO_2. On the other hand, rGT and rGT/FP have obvious enhanced absorption in the visible light region. Furthermore, a red shift could be detected on the spectra of rGT and rGT/FP. These results indicated that the modification with rGO could enhance the PC degradation activity of TiO_2 (Min *et al.* 2017).

Photoelectrochemical properties

Figure 4(a) shows the transient photocurrent response of TiO_2/FP and rGT/FP photoelectrodes, under UV-light irradiation without applied bias. The rGT/FP owns a higher photocurrent than that of TiO_2/FP. The photocurrent response of rGT/FP photocatalyst electrodes is greatly enhanced by 3.5 fold, compared to the pristine TiO_2. This result indicates the improved charge separation and transportation efficiency of the rGT/FP photoelectrode, because the rGO enhanced the light absorption and accelerated the transfer of photogenerated electrons. Figure 4(b) shows the photocurrent of TiO_2/FP and rGT/FP in 0.1 M Na_2SO_4 electrolyte under a bias from −1.0 V to 1.0 V (vs Ag/AgCl), using the UV light as the illuminant. The saturated photocurrent of rGT/FP is higher than that of pure TiO_2/FP, indicating that there are more photoexcited electrons on the rGT/FP electrode's flow to the cathode (Wang *et al.* 2012; Zhang *et al.* 2012; Zhou *et al.* 2014).

PEC decolorization

In order to investigate the catalytic performances of the TiO_2/FP and rGT/FP photoelectrodes, the decolorization of MB in the supporting electrolyte was conducted in terms of the PC, electrocatalytic (EC), and PEC treatments.

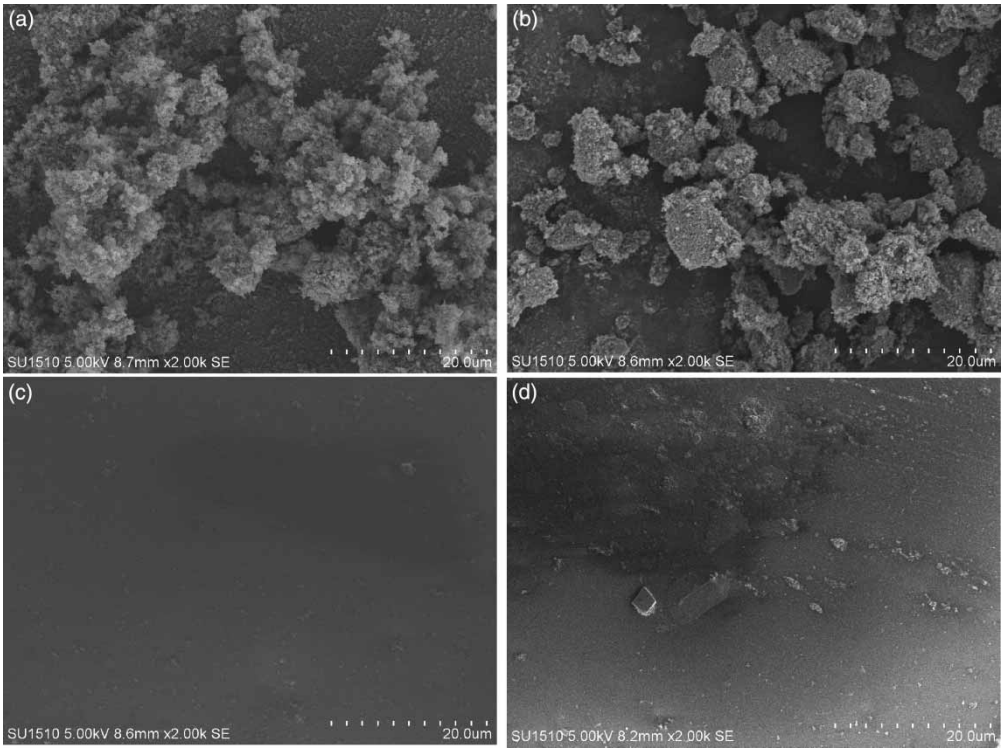

Figure 1 | SEM images of (a) pure TiO_2 and (b) rGT, (c) TiO_2/FP and (d) rGT/FP.

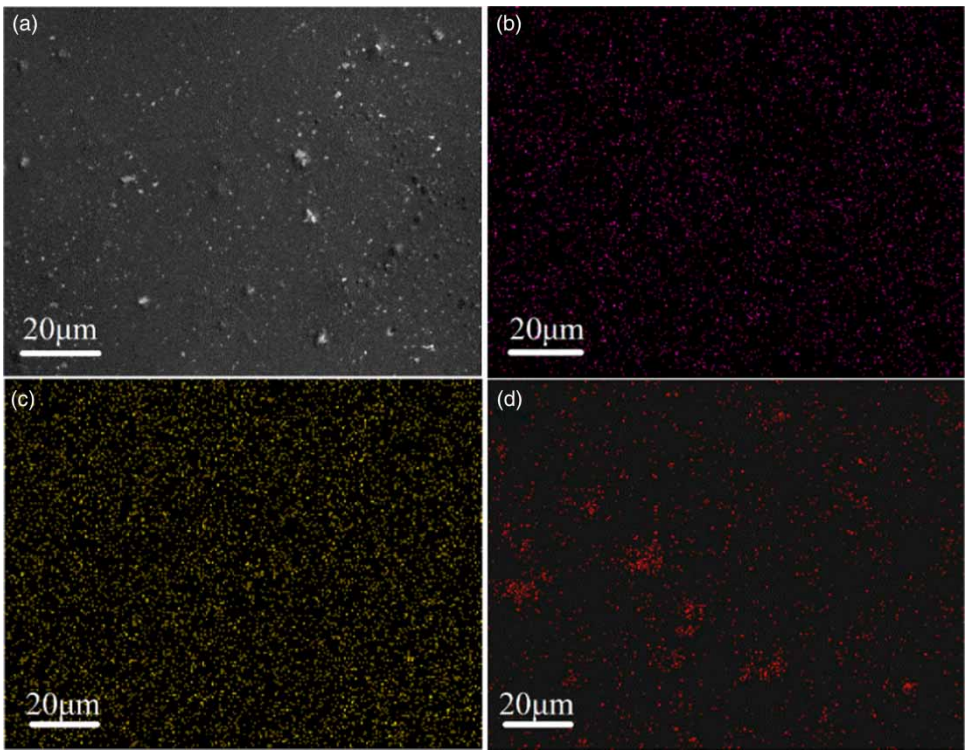

Figure 2 | EDS mapping images of the elements on (a) rGT/FP: (b) O, (c) C and (d) Ti.

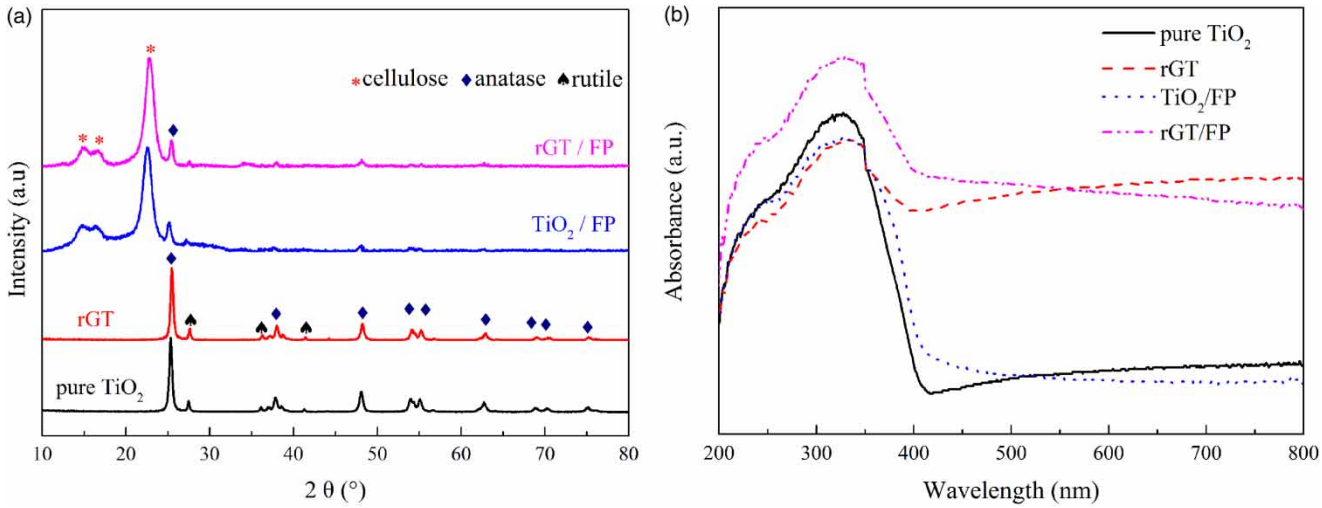

Figure 3 | (a) XRD patterns and (b) UV-Vis DRS of pure TiO_2, rGT, TiO_2/FP and rGT/FP.

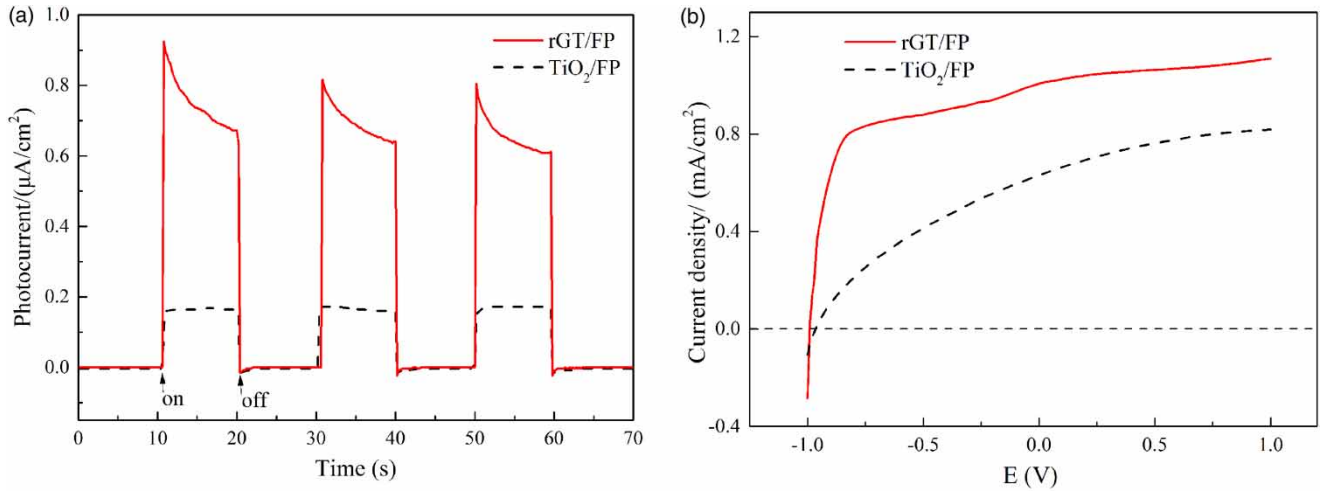

Figure 4 | (a) Transient photocurrent response of TiO_2/FP and rGT/FP photoelectrodes in 0.1 M Na_2SO_4 at pH = 7.0; (b) variations of photocurrent density vs. the bias voltage from −1.0 V to 1.0 V.

In this work, two basic conditions of applied voltages and initial dye concentrations were investigated to understand their effects on the decolorization efficiency of the EC process.

The EC decolorization performances using the photoelectrodes of TiO_2/FP and rGT/FP are firstly assessed at various external biases in darkness. It is of note that the EC decolorization rates using rGT/FP are much higher than that using TiO_2/FP. Furthermore, as shown in Figure 5(a), the EC decolorization rates on the rGT/FP photoelectrode, after 60 min treatment, are 15.36%, 43.88%, 74.23% and 82.88% at applied voltages of 4, 8, 12 and 16 V, respectively. This result indicated that the EC decolorization efficiency can be significantly impacted by the applied voltage, because the applied voltage can reduce the recombination rate of e^- and h^+ pairs. However, the increment declined sharply as the applied voltage exceeded 12 V. This phenomenon is caused by the recombination reaction between the e^- derived from external voltage and h^+ formed on the TiO_2, which resulted in the consumption of active species and the decrease of the MB decolorization rate (Kim *et al.* 2017). Therefore, the applied voltage of 12 V was chosen for further experiments.

MB solution with concentrations of 5, 10, 15 and 20 mg/L was used to investigate the influence of dye concentration on decolorization efficiency. As shown in Figure 5(b), the decolorization rate decreases with increasing dye concentration. The decolorization processes can be divided into

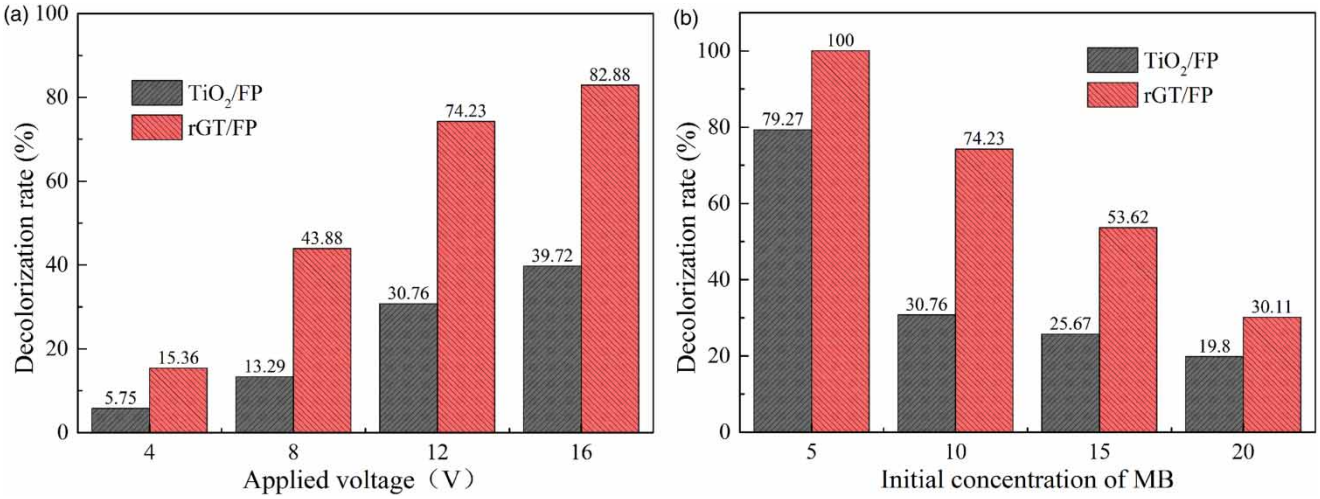

Figure 5 | (a) Decolorization rate of MB using TiO_2/FP and rGT/FP photoelectrodes, under various applied voltages of 4, 8, 12 and 16 V; (b) decolorization rate of TiO_2/FP and rGT/FP photoelectrodes, at different initial MB concentrations of 5, 10, 15 and 20 mg/L.

the two main steps, including dye diffusion from the solution to the surface of the electrode, and dye degradation by the electrochemical reaction. At low dye concentrations, the decolorization rate was mainly controlled by the diffusion process, because the electrochemical reaction was faster than the diffusion rate and could rapidly degrade the dye molecules. As the concentration increased, more dye molecules could diffuse to the surface of the electrode and could not be degraded in time, resulting in a lower degradation rate (Rajkumar *et al.* 2007).

The decolorization capabilities of the TiO_2/FP and rGT/FP were also evaluated with the PC decolorization process. As shown in Figure 6(a), the TiO_2/FP achieved PC decolorization of 15.34% within 60 min under UV irradiation, while rGT/FP presented PC decolorization of 29.26%. This result indicated that the incorporated rGO increases absorption of visible light, and also acts like a charge separator to reduce the recombination rate of 'electron-hole' pairs (Garrafa-Galvez *et al.* 2019), which is consistent with the UV-Vis diffuse reflectance spectra in Figure 3(b). The enhancement of the decolorization rate can also be observed in the EC and PEC decolorization processes, using the TiO_2/FP and rGT/FP photoelectrodes, respectively, as shown in Figure 6(b) and 6(c). The decolorization efficiency using the rGT/FP photoelectrode is much higher than that of the TiO_2/FP photoelectrode. There are two main reasons for the enhancement of the PEC decolorization rate: (1) the electrical conductivity of rGO can accelerate the overall electron speed of the photoelectrode; and (2) the narrow band gap of rGO benefits the transfer of photogenerated electrons from the valence band to the conduction band (Zhai *et al.* 2013). Therefore, the recombination rate of 'electron-hole' pairs is decreased, resulted in the improvement of the decolorization efficiency (Wang *et al.* 2012; Min *et al.* 2017).

When light photons (hv) of sufficient energy are incident on TiO_2, the process in Equation (1) occurs:

$$TiO_2 + hv \rightarrow e^- + h^+ \quad (1)$$

These charges are capable of interacting with species in the heterogeneous system. For example, h^+ are powerful oxidants that can react with the organics and water molecules that are absorbed onto the surface of the photoelectrode. Furthermore, the trapped holes are indicated to undergo one-electron oxidation step with water molecules to generate highly oxidising hydroxyl radicals. Equations (2)–(4) depict the interaction of photogenerated holes with organics and water molecules.

$$MB + h^+ \rightarrow \text{product} \quad (2)$$

$$H_2O + h^+ \rightarrow OH^\bullet + H^+ \quad (3)$$

$$OH^- + h^+ \rightarrow OH^\bullet \quad (4)$$

The electrons at the conduction band can interact with adsorbed or dissolved oxygen in the reaction system to form superoxide ions, as shown in Equation (5). The superoxide ions are also known to possess considerable oxidizing power (Equation (6)). Further reactions can take place between the various species in the mixture as depicted by

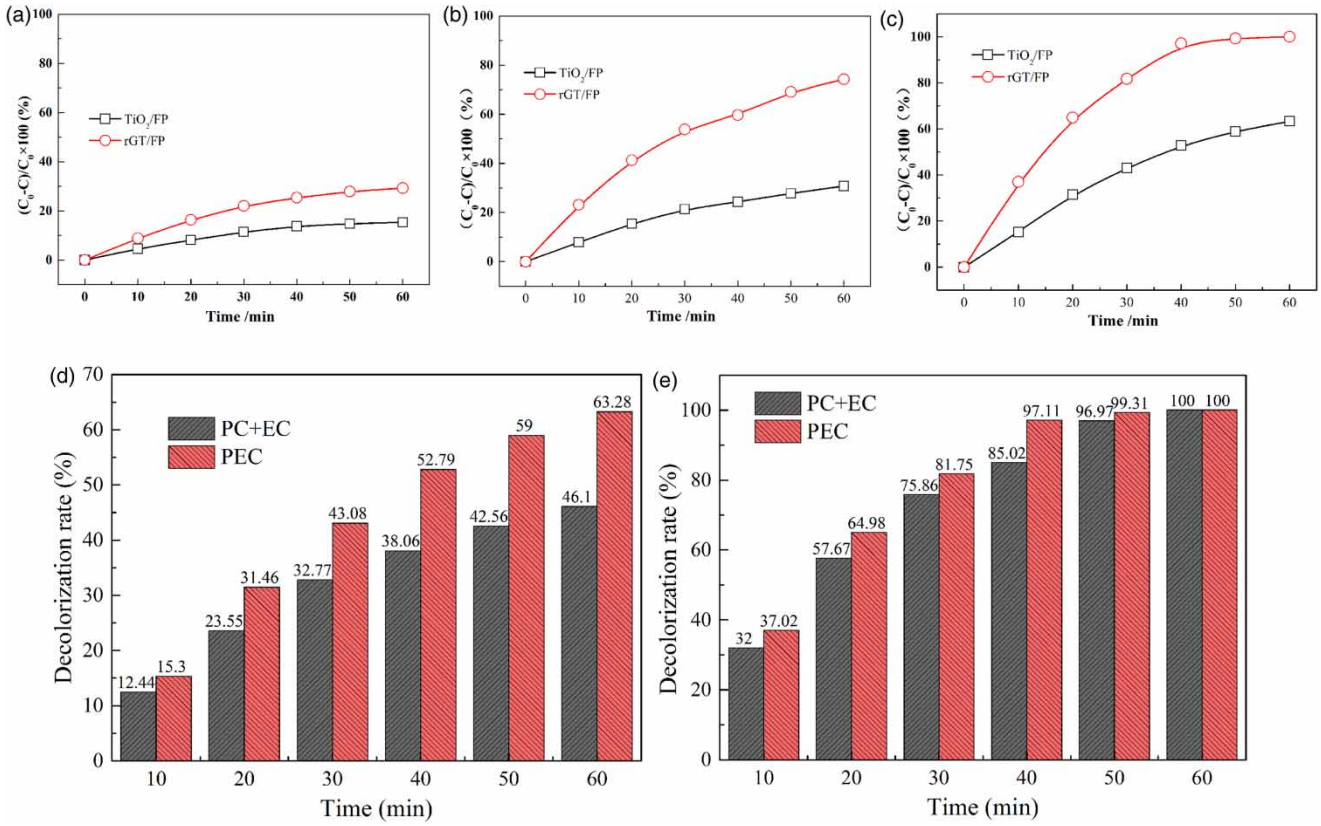

Figure 6 | Decolorization rate obtained during the treatment of 10 mg/L MB over the TiO_2/FP and rGO/FP photoelectrodes by the different process of (a) PC (under UV irradiation), (b) EC (with an applied voltage of 12 V), (c) PEC (under irradiation and a 12 V applied voltage), and PEC process of MB over the (d) TiO_2/FP and (e) rGO/FP photoelectrodes.

Equations (7) and (8).

$$e^- + O_2 \rightarrow O_2^{\bullet -} \quad (5)$$

$$O_2^{\bullet -} + H^+ \rightarrow OOH^{\bullet} \quad (6)$$

$$OOH^{\bullet} + H^+ + e^- \rightarrow H_2O_2 \quad (7)$$

$$H_2O_2 + h\nu \rightarrow 2\,OH^{\bullet} \quad (8)$$

Notably, Cl^- in the electrolyte also plays an important role in the reaction (Olvera-Rodríguez *et al.* 2019). The active chlorine species are formed from oxidation of Cl^- to dissolved Cl_2 at the photoelectrode via reaction (9), followed by hydrolysis to hypochlorous acid (HClO) via reaction (10).

$$2Cl^- \rightarrow Cl_{2(aq)} + 2e^- \quad (9)$$

$$Cl_{2(aq)} + H_2O \rightarrow HClO + Cl^- + H^+ \quad (10)$$

Most importantly, PEC treatment using the rGT/FP photoelectrode achieved the highest decolorization rate (almost 100% decolorization of MB within 50 min). Furthermore, as shown in Figure 6(d) and 6(e), the summary decolorization efficiency of MB by EC + PC treatment is lower than that using PEC treatment, which indicated the synergetic effect in the PEC process. The corresponding parameters, k and R^2 (regression coefficients) of MB decolorization by the rGT/FP photoelectrode under the PC, EC and PEC processes are listed in Table S1 (Supplementary Material). The rate constants of the decolorization of MB over the PC, EC and the PEC activity are determined to be 0.0051, 0.0215 and 0.1152 min^{-1}, respectively. Apparently, the kinetic constant of the PEC process is about 22-fold and 5-fold that of the PC process and EC process, respectively, which further demonstrates the enhanced decolorization efficiency from using PEC process.

The UV-Vis absorbance spectra of MB solution during PEC decolorization were measured and are shown in Figure S1 (Supplementary Material). The original MB solution before PEC decolorization exhibits two defined UV-Vis absorption peaks at 292 nm and 664 nm, respectively. The peak observed at 292 nm was ascribed to the aromatic rings in the MB molecules, and the peak at 664 nm was

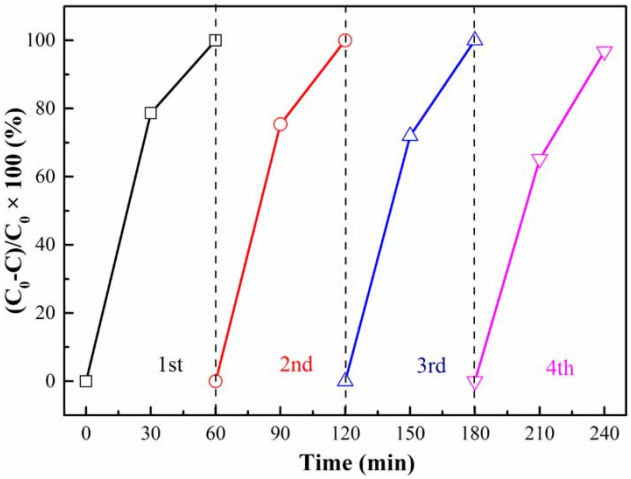

Figure 7 | PEC decolorization of MB solution using rGT/FP photoelectrodes for four cycles.

attributed to the dimethylamino structure of MB. During the degradation process, the absorption peaks decrease with increasing PEC time. For a PEC time of 60 min, these two peaks had completely disappeared, and no new peaks appeared in the visible region, which indicated that complete decolorization of MB was achieved.

Recyclability is another essential factor to evaluate the photoelectrode. The stability of the rGT/FP photoelectrode was investigated by recycling the PEC decolorization processes. As shown in Figure 7, no obvious decrease was observed in the PEC activity after the rGT/FP photoelectrode had been used for four cycles. The electrochemical performance of rGT/FP was also tested to measure its stability; the results are shown in Figure S2 (Supplementary Material). The excellent recyclability is mainly due to the film-making materials used for preparing the rGT/FP photoelectrode. As a typical cellulose ether, ethyl cellulose has a similar structure to cellulose, which can cohere with filter paper by hydrogen bonds. In consequence, ethyl cellulose and ethyl alcohol film provide the mechanical support for the filter paper and also improve its durability (Philip *et al.* 2008). Table S2 in the Supplementary Material presents the optical images of the rGT/FP photoelectrode in four cycles. There was no obvious changes that could be observed, implying the excellent stability of the rGT/FP photoelectrode.

CONCLUSIONS

In conclusion, the hybrid rGT/FP photoelectrode based on filter paper was prepared and used for PEC decolorization of MB. Compared with the TiO_2/FP photoelectrode, the rGT/FP photoelectrode shows enhanced PEC decolorization efficiency. The UV-Vis reflectance spectra reveal that the incorporation of TiO_2 with rGO can extend the absorption range to the visible region. The photocurrent and linear sweep voltage results indicate that the enhanced PEC decolorization efficiency using the rGT/FP photoelectrode is attributed to the existence of rGO sheets. Furthermore, the PEC process exhibits a synergistic effect, in which the decolorization efficiency of MB by PEC treatment is higher than the summary of EC and PC treatment. This work provides a novel strategy for developing cost-effective and efficient PEC materials for decolorization of organic pollutants.

ACKNOWLEDGEMENTS

This work was financially supported by the National Natural Science Foundation of China (No. 51903107, 51803076), the Postdoctoral Science Foundation of Jiangsu Province (1701012B), the China Postdoctoral Science Foundation (2017M611696, 2018M63223), the Natural Science Foundation of Jiangsu Province (No. BK20190619, BK20180629), and the Open Project Program of Fujian Key Laboratory of Novel Functional Textile Fibers and Materials (Minjiang University), China (No. FKLTFM1809).

SUPPLEMENTARY MATERIAL

The Supplementary Material for this paper is available online at https://dx.doi.org/10.2166/wst.2019.425.

REFERENCES

Almeida, L. C. & Zanoni, M. V. B. 2014 Decoration of Ti/TiO_2 nanotubes with Pt nanoparticles for enhanced UV-Vis light absorption in photoelectrocatalytic process. *Journal of the Brazilian Chemical Society* **25**, 579–588.

Bolotin, K. I., Sikes, K. J., Jiang, Z., Klima, M., Fudenberg, G., Hone, J., Kim, P. & Stormer, H. L. 2008 Ultrahigh electron mobility in suspended graphene. *Solid State Communications* **146**, 351–355.

Chen, C., Ma, W. & Zhao, J. 2010 Semiconductor-mediated photodegradation of pollutants under visible-light irradiation. *Chemical Society Reviews* **39**, 4206–4219.

Chen, F., An, W., Yao, L., Liang, Y. & Cui, W. 2018 Fabricating 3D porous PANI/TiO_2–graphene hydrogel for the enhanced UV-light photocatalytic degradation of BPA. *Applied Surface Science* **427**, 123–132.

Dai, G., Yu, J. & Liu, G. 2011 Synthesis and enhanced visible-light photoelectrocatalytic activity of *p–n* junction BiOI/TiO_2 nanotube arrays. *The Journal of Physical Chemistry C* **115**, 7339–7346.

Du, X., Skachko, I., Barker, A. & Andrei, E. Y. 2008 Approaching ballistic transport in suspended graphene. *Nature Nanotechnology* **3**, 491–495.

Garrafa-Galvez, H. E., Alvarado-Beltran, C. G., Almaral-Sanchez, J. L., Hurtado-Macias, A., Garzon-Fontecha, A. M., Logue, P. A. & Castro-Beltran, A. 2019 Graphene role in improved solar photocatalytic performance of TiO_2-RGO nanocomposite. *Chemical Physics* **521**, 35–43.

Ghasemi, S., Esfandiar, A., Setayesh, R., Habibiyangjeh, A. & Zad, I. 2013 Synthesis and characterization of TiO_2-graphene nanocomposites modified with noble metals as a photocatalyst for degradation of pollutants. *Applied Catalysis A: General* **462–463**, 82–90.

Guo, H., Jiang, N., Wang, H., Shang, K., Lu, N., Li, J. & Wu, Y. 2019 Enhanced catalytic performance of graphene-TiO_2 nanocomposites for synergetic degradation of fluoroquinolone antibiotic in pulsed discharge plasma system. *Applied Catalysis B: Environmental* **248**, 552–566.

Hoffmann, M. R., Choi, W. & Bahnemann, D. W. 1995 Environmental applications of semiconductor photocatalysis. *Chemical Reviews* **95**, 69–96.

Kim, D. H. & Anderson, M. A. 1994 Photoelectrocatalytic degradation of formic acid using a porous titanium dioxide thin-film electrode. *Environmental Science & Technology* **28**, 479–483.

Kim, S.-R., Ali, I. & Kim, J.-O. 2017 Phenol degradation using an anodized graphene-doped TiO_2 nanotube composite under visible light. *Applied Surface Science* **477**, 71–78.

Koketsu, T., Ma, J., Morgan, B. J., Body, M., Legein, C., Dachraoui, W., Giannini, M., Demortière, A., Salanne, M. & Dardoize, F. 2017 Reversible magnesium and aluminium ions insertion in cation-deficient anatase TiO_2. *Nature Materials* **16**, 1142–1148.

Li, B., Cao, X., Ong, H. G., Cheah, J. W., Zhou, X., Yin, Z., Li, H., Wang, J., Boey, F. & Huang, W. 2010 All-carbon electronic devices fabricated by directly grown single-walled carbon nanotubes on reduced graphene oxide electrodes. *Advanced Materials* **22**, 3058–3061.

Liang, Y., Wang, H., Casalongue, H. S., Chen, Z. & Dai, H. 2010 TiO_2 nanocrystals grown on graphene as advanced photocatalytic hybrid materials. *Nano Research* **3**, 701–705.

Liao, P. & Carter, E. A. 2013 New concepts and modeling strategies to design and evaluate photo-electro-catalysts based on transition metal oxides. *Chemical Society Reviews* **42**, 2401–2422.

Lindblad, R., Cappel, U. B., O'Mahony, F. T., Siegbahn, H., Johansson, E. M., Haque, S. A. & Rensmo, H. 2014 Energy level alignment in TiO_2/metal sulfide/polymer interfaces for solar cell applications. *Physical Chemistry Chemical Physics* **16**, 17099–17107.

Litke, A., Weber, T., Hofmann, J. P. & Hensen, E. J. M. 2016 Bottlenecks limiting efficiency of photocatalytic water reduction by mixed Cd-Zn sulfides/Pt-TiO_2 composites. *Applied Catalysis B: Environmental* **198**, 16–24.

Liu, X., Pan, L., Zhao, Q., Lv, T., Zhu, G., Chen, T., Lu, T., Sun, Z. & Sun, C. 2012 UV-assisted photocatalytic synthesis of ZnO–reduced graphene oxide composites with enhanced photocatalytic activity in reduction of Cr (VI). *Chemical Engineering Journal* **183**, 238–243.

Mao, L., Wang, Y., Zhong, Y., Ning, J. & Hu, Y. 2013 Microwave-assisted deposition of metal sulfide/oxide nanocrystals onto a 3D hierarchical flower-like TiO_2 nanostructure with improved photocatalytic activity. *Journal of Materials Chemistry A* **1**, 8101–8104.

Min, S., Hou, J., Lei, Y., Ma, X. & Lu, G. 2017 Facile one-step hydrothermal synthesis toward strongly coupled TiO_2/graphene quantum dots photocatalysts for efficient hydrogen evolution. *Applied Surface Science* **396**, 1375–1382.

Olvera-Rodríguez, I., Hernández, R., Medel, A., Guzmán, C., Escobar-Alarcón, L., Brillas, E., Sirés, I. & Esquivel, K. 2019 TiO_2/Au/TiO_2 multilayer thin-film photoanodes synthesized by pulsed laser deposition for photoelectrochemical degradation of organic pollutants. *Separation and Purification Technology* **224**, 189–198.

Philip, A. K., Pathak, K. & Shakya, P. 2008 Asymmetric membrane in membrane capsules: a means for achieving delayed and osmotic flow of cefadroxil. *European Journal of Pharmaceutics and Biopharmaceutics* **69**, 658–666.

Qin, G., Wu, Q., Sun, Z., Wang, Y., Luo, J. & Xue, S. 2012 Enhanced photoelectrocatalytic degradation of phenols with bifunctionalized dye-sensitized TiO_2 film. *Journal of Hazardous Materials* **199–200**, 226–232.

Rajkumar, D., Song, B. J. & Kim, J. G. 2007 Electrochemical degradation of Reactive Blue 19 in chloride medium for the treatment of textile dyeing wastewater with identification of intermediate compounds. *Dyes and Pigments* **72**, 1–7.

Rajkumar, K., Vairaselvi, P., Saravanan, P., Vinod, V. T. P., Černík, M. & Kumar, R. T. R. 2015 Visible-light-driven SnO_2/TiO_2 nanotube nanocomposite for textile effluent degradation. *RSC Advances* **5**, 20424–20431.

Ren, M., Horn, H. & Frimmel, F. H. 2017 Aggregation behavior of TiO_2 nanoparticles in municipal effluent: influence of ionic strengthen and organic compounds. *Water Research* **123**, 678–686.

Sánchez-Rodríguez, D., Medrano, M. G. M., Remita, H. & Escobar-Barrios, V. 2018 Photocatalytic properties of BiOCl-TiO_2 composites for phenol photodegradation. *Journal of Environmental Chemical Engineering* **6**, 1601–1612.

Sathishkumar, K., Sathiyaraj, S., Parthipan, P., Akhil, A., Murugan, K. & Rajasekar, A. 2017 Electrochemical decolorization of methyl red by RuO_2-IrO_2-TiO_2 electrode and biodegradation with *Pseudomonas stutzeri* MN1 and *Acinetobacter baumannii* MN3: an integrated approach. *Chemosphere* **183**, 204–211.

Sieland, F., Schneider, J. & Bahnemann, D. W. 2018 Photocatalytic activity and charge carrier dynamics of TiO_2 powders with a binary particle size distribution. *Physical Chemistry Chemical Physics* **20**, 8119–8132.

Smirnova, N., Petrik, I., Vorobets, V., Kolbasov, G. & Eremenko, A. 2017 Sol-gel synthesis, photo- and electrocatalytic properties of mesoporous TiO_2 modified with transition metal ions. *Nanoscale Research Letters* **12**, 239.

Subramonian, W., Wu, T. Y. & Chai, S. P. 2017 Photocatalytic degradation of industrial pulp and paper mill effluent using synthesized magnetic Fe_2O_3-TiO_2: treatment efficiency and characterizations of reused photocatalyst. *Journal of Environmental Management* **187**, 298–310.

Takle, S. P., Apine, O. A., Ambekar, J. D., Landge, S. L., Bhujbal, N. N., Kale, B. B. & Sonawane, R. S. 2019 Solar-light-active mesoporous Cr–TiO_2 for photodegradation of spent wash: an in-depth study using QTOF LC-MS. *RSC Advances* **9**, 4226–4238.

Tao, W., Da, H., Zhi, Y., Xu, S., He, G., Li, X., Hu, N., Yin, G., He, D. & Zhang, L. 2016 A review on graphene-based gas/vapor sensors with unique properties and potential applications. *Nano-Micro Letters* **8**, 95–119.

Wang, D., Li, X., Chen, J. & Tao, X. 2012 Enhanced photoelectrocatalytic activity of reduced graphene oxide/TiO_2 composite films for dye degradation. *Chemical Engineering Journal* **198–199**, 547–554.

Wang, H., Liang, Y., Liu, L., Hu, J. & Cui, W. 2018 Highly ordered TiO_2 nanotube arrays wrapped with g-C_3N_4 nanoparticles for efficient charge separation and increased photoelectrocatalytic degradation of phenol. *Journal of Hazardous Materials* **344**, 369–380.

Wei, D., Wu, B., Guo, Y., Yu, G. & Liu, Y. 2013 Controllable chemical vapor deposition growth of few layer graphene for electronic devices. *Accounts of Chemical Research* **46**, 106–115.

Williams, G., Seger, B. & Kamat, P. V. 2008 TiO_2-graphene nanocomposites. UV-assisted photocatalytic reduction of graphene oxide. *ACS Nano* **2**, 1487–1491.

Xiang, Q., Yu, J. & Jaroniec, M. 2011 Enhanced photocatalytic H-2-production activity of graphene-modified titania nanosheets. *Nanoscale* **3**, 3670–3678.

Yan, Y., Yu, Y., Huang, S., Yang, Y., Yang, X., Yin, S. & Cao, Y. 2017 Adjustment and matching of energy band of TiO_2-based photocatalysts by metal ions (Pd, Cu, Mn) for photoreduction of CO_2 into CH4. *Journal of Physical Chemistry C* **121**, 1089–1098.

Zhai, C., Zhu, M., Ren, F., Yao, Z., Du, Y. & Yang, P. 2013 Enhanced photoelectrocatalytic performance of titanium dioxide/carbon cloth based photoelectrodes by graphene modification under visible-light irradiation. *Journal of Hazardous Materials* **263**, 291–298.

Zhang, H., Lv, X., Li, Y., Wang, Y. & Li, J. 2009 P25-graphene composite as a high performance photocatalyst. *ACS Nano* **4**, 380–386.

Zhang, Y., Tang, Z. R., Fu, X. & Xu, Y. J. 2010 TiO_2-graphene nanocomposites for gas-phase photocatalytic degradation of volatile aromatic pollutant: is TiO_2-graphene truly different from other TiO_2-carbon composite materials? *ACS Nano* **4**, 7303–7314.

Zhang, Z., Yu, Y. & Wang, P. 2012 Hierarchical top-porous/bottom-tubular TiO_2 nanostructures decorated with Pd nanoparticles for efficient photoelectrocatalytic decomposition of synergistic pollutants. *ACS Applied Materials & Interfaces* **4**, 990–996.

Zhang, C., Yu, H., Li, Y., Gao, Y., Zhao, Y., Song, W., Shao, Z. & Yi, B. 2013 Supported noble metals on hydrogen-treated TiO_2 nanotube arrays as highly ordered electrodes for fuel cells. *Chemsuschem* **6**, 659–666.

Zhang, J., Zhang, L., Ma, X. & Ji, Z. 2018 A study of constructing heterojunction between two-dimensional transition metal sulfides (MoS_2 and WS_2) and (101), (001) faces of TiO_2. *Applied Surface Science* **430**, 424–437.

Zhou, W., Li, W., Wang, J.-Q., Qu, Y., Yang, Y., Xie, Y., Zhang, K., Wang, L., Fu, H. & Zhao, D. 2014 Ordered mesoporous black TiO_2 as highly efficient hydrogen evolution photocatalyst. *Journal of the American Chemical Society* **136**, 9280–9283.

First received 10 July 2019; accepted in revised form 5 December 2019. Available online 24 December 2019